

DESIGN OF A COMPUTATIONAL-FLUID-DYNAMICS TOOL FOR THE SIMULATION OF PRE-SPECIFIED FIRE SCENARIOS IN ENCLOSURES

Aram Amouzandeh*, Shankar Shrestha*, Matthias Zeiml*
and Roman Lackner†

*Institute for Mechanics of Materials and Structures
Vienna University of Technology, Karlsplatz 13, 1040 Vienna, Austria
e-mail: {aram.amouzandeh,shankar.shrestha,matthias.zeiml}@tuwien.ac.at

†Material-Technology Innsbruck
University of Innsbruck, Technikerstraße 13, 6020 Innsbruck, Austria
e-mail: roman.lackner@uibk.ac.at

Key words: OpenFOAM, Fire, Buoyancy-augmentation, Radiation, Combustion

Abstract. *In the present work, Computational Fluid Dynamics (CFD) is employed to determine the thermal loading of structures during fire accidents. CFD-analyses allow to determine the temperature distribution at the surface of the load-carrying structure replacing the commonly-used standard temperature-time curves of design codes. The respective CFD code is designed to reproduce a turbulent buoyancy-driven flow induced by the combustion process, accounting for conductive, convective, and radiative heat transfer. In order to meet these demands, a buoyancy-augmented $k-\varepsilon$ model as well as suitable models covering radiation and combustion are implemented in OpenFOAM's `chtMultiRegionFoam` solver. Regarding turbulence, the standard $k-\varepsilon$ model is modified based on the Generalized Gradient Diffusion Hypothesis (GGDH) in order to account for turbulence production due to buoyancy effects. Furthermore, two radiation models implemented in OpenFOAM (i.e., $P1$ and Finite Volume Discrete Ordinate Method ($fvDOM$)) are investigated by means of selected benchmark tests. To capture the phenomenon of burning gases, an appropriate combustion model is studied and introduced into the code.*

Nomenclature

a	absorption coefficient (1/m)	R	reaction rate (kg/(m ³ s))
B_0	buoyancy added at the source (m ⁴ /s ³)	r	radial coordinate (m); aspect ratio (1)
c_p	specific heat capacity (J/(kg K))	\mathbf{s}	direction vector (m)
D	diameter; distance between walls (m);	s	stoichiometric air/fuel mass ratio (1)
D^*	characteristic plume diameter (m)	T	temperature (K)
\mathcal{D}	mass diffusivity (m ² /s)	Tu	turbulent intensity (1)
g	gravitational acceleration (m/s ²)	u_j	velocity component (m/s)
Δh_C	heat of combustion (J/kg)	u	radial velocity (m/s)
G	turbulence production due to shear (W/m ³); incident radiative heat flux (W/m ²)	w	axial velocity (m/s)
I	radiative intensity (W/m ²)	X_r	radiative fraction (1)
k	spec. turbulent kinetic energy (m ² /s ²)	x_j	coordinate (m)
l_m	turbulent mixing length (m)	\mathbf{x}	position vector (m)
L_M	Morton length scale (m)	Y	mass fraction (1)
M_0	momentum added at the source (m ⁴ /s ²)	y_0	horizontal extension of rectangular enclosure (m)
p	pressure (Pa)	Z	mixture fraction (1)
P	turbulence production due to buoyancy (W/m ³)	z	axial coordinate (m)
Q	burning rate (W)	z_0	vertical extension of rectangular enclosure (m); virtual source location (m)
q_C	combustion heat source term (W/m ³)		
\mathbf{q}_R	radiative heat flux vector (W/m ²)		

Greek symbols

β	thermal expansion coefficient (1/K)
ε	turbulent dissipation rate (m ² /s ³)
Φ_b	dimensionless temperature (1)
η	similarity variable (1)
μ	viscosity (Pa s)
μ_t	eddy viscosity (Pa s)
ρ	density (kg/m ³)
σ_{SB}	Stefan-Boltzmann constant (W/(m ² K ⁴))
Ω	solid angle (1)
κ	optical thickness (1)
Ψ_b	dimensionless heat flux (1)

Subscripts

0	source condition
∞	ambient condition
b	black body
f	fuel
j, k	coordinate index
o	oxidizer
w	wall

Superscripts

$\bar{\bullet}$	Reynolds-average
\bullet'	fluctuation

1 INTRODUCTION

Fire accidents in recent years caused numerous casualties as well as an immense economic loss, making a thorough investigation of such incidents necessary. In the present work, Computational Fluid Dynamics (CFD) is employed to determine the thermal loading of structures in case of fire. Starting with the heat release rate (HRR) of the fire source, the temperature distribution at the surface of the load-carrying structure is determined by CFD-analyses (see Figure 1), replacing the commonly-used standard temperature-time curves of design codes.

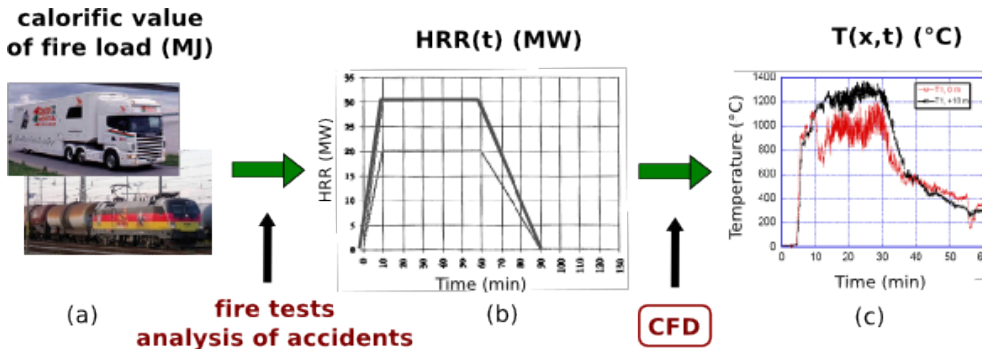


Figure 1: Application of CFD for the simulation of fire: (a) type of fire load, (b) evolution of HRR, and (c) evolution of surface temperature determined by means of CFD

Different CFD-codes designed to simulate fires in enclosures were studied [7], a pre-selection according to specified criteria suggested the two codes *Fire Dynamics Simulator (FDS)* and *OpenFOAM* for further investigation. This paper focuses on the development of an appropriate fire-analysis code in OpenFOAM. The obtained numerical results are compared with analytical/experimental data.

The code has to reproduce a turbulent buoyancy-driven flow induced by the combustion process, accounting for conductive, convective, and radiative heat transfer. Therefore, a buoyancy-augmented $k-\varepsilon$ model as well as suitable models covering radiation and combustion are implemented in OpenFOAM's *chtMultiRegionFoam* solver. In Section 2, the standard $k-\varepsilon$ model is modified by introducing additional source terms in the $k-\varepsilon$ system in order to account for turbulence production due to buoyancy effects. Section 3 deals with the two radiation models implemented in OpenFOAM, i.e., *P1* and *Finite Volume Discrete Ordinate Method (fvDOM)*. In order to capture the phenomenon of burning gases, an appropriate combustion model is studied in Section 4.

2 THE BUOYANCY-AUGMENTED $k-\varepsilon$ TURBULENCE MODEL

The driving forces of fire-induced fluid flows mainly come from buoyancy effects due to large density differences. As a result, the influence of buoyancy on turbulence production plays a vital role for the prediction of heat transfer in case of fire. It is well known that the most-commonly used turbulence model in CFD, the standard $k-\varepsilon$, model strongly

underestimates the effects of buoyancy on the turbulence production. In order to overcome this problem, a so-called buoyancy-augmentation is incorporated into the standard k - ε model, characterised by additional source terms in the transport equations of k and ε to consider the turbulence production due to buoyancy. The calculation of the new source terms is based on the *Generalized Gradient Diffusion Hypothesis (GGDH)* studied and recommended for fire simulations in [12]. In the present work, numerical results produced with the modified turbulence model are compared with measurements on a round turbulent buoyant plume presented in [10].

2.1 Governing equations of the buoyancy-modified k - ε model

The transport equations of the k - ε system for a buoyancy-augmented model are deduced from the standard k - ε model, yielding

$$\frac{\partial}{\partial t} (\bar{\rho}k) + \frac{\partial}{\partial x_j} (\bar{\rho}k\bar{u}_j) = \frac{\partial}{\partial x_j} \left[\left(\mu + \frac{\mu_t}{\sigma_k} \right) \frac{\partial k}{\partial x_j} \right] + G + P - \bar{\rho}\varepsilon \quad (1)$$

and

$$\frac{\partial}{\partial t} (\bar{\rho}\varepsilon) + \frac{\partial}{\partial x_j} (\bar{\rho}\varepsilon\bar{u}_j) = \frac{\partial}{\partial x_j} \left[\left(\mu + \frac{\mu_t}{\sigma_\varepsilon} \right) \frac{\partial \varepsilon}{\partial x_j} \right] + C_1 \frac{\varepsilon}{k} G + C_1 \frac{\varepsilon}{k} (1 - C_3) P - C_2 \bar{\rho} \frac{\varepsilon^2}{k}, \quad (2)$$

where additional source terms including the turbulence production due to buoyancy-effects, P , have been added to the respective equations of the standard k - ε model. P is given by

$$P = \frac{\overline{\rho'u_j'}}{\bar{\rho}} \left(\frac{\partial \bar{p}}{\partial x_j} + \rho_\infty g_j \right). \quad (3)$$

Based on the GGDH studied in [12], reading

$$\overline{\rho'u_j'} = -\frac{3}{2} \frac{C_\mu}{\sigma_t} \frac{k}{\varepsilon} \left(\overline{u_j'u_k'} \frac{\partial \bar{p}}{\partial x_k} \right), \quad (4)$$

and neglecting the pressure derivative since $|\partial \bar{p} / \partial x_j| \ll \rho_\infty g_j$, P can be expressed as

$$P = -\frac{3}{2} g_j \frac{C_\mu}{\sigma_t} \frac{\rho_\infty}{\bar{\rho}} \frac{k}{\varepsilon} \left(\overline{u_j'u_k'} \frac{\partial \bar{p}}{\partial x_k} \right). \quad (5)$$

Within the analyses, the following model constants are used: $C_\mu = 0.09$, $C_1 = 1.44$, $C_2 = 1.92$, $C_3 = 0.8$, $\sigma_k = 1$, $\sigma_\varepsilon = 1.3$, and $\sigma_t = 0.85$.

2.2 Application – round turbulent buoyant plume

2.2.1 Experimental layout

The numerical results obtained with OpenFOAM applying both the standard and the buoyancy-augmented k - ε model are compared with the experimental findings presented in [10] for an isolated, round turbulent plume (see Figure 2).

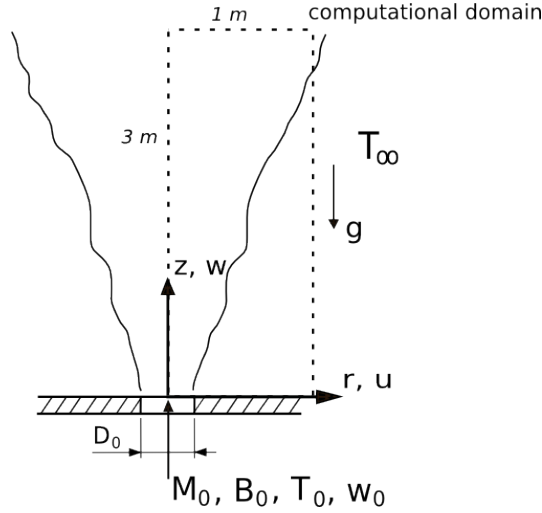


Figure 2: Nomenclature for the plume experiment

The considered experiments [13] are characterised by hot air ($T_0 = 573$ K) entering a quiescent environment ($T_\infty = 302$ K) at a velocity $w_0 = 0.67$ m/s through a round opening with a diameter $D_0 = 0.0635$ m. Velocity and temperature profiles were measured at various locations in the area of self-preserving conditions of the plume. In [10], it is reported that self-preserving conditions are reached at $z/L_M > 5$, where z denotes the vertical distance from the source and L_M the Morton length scale, given by

$$L_M = \frac{M_0^{\frac{3}{4}}}{B_0^{\frac{1}{2}}}. \quad (6)$$

The value of L_M depends on the two important parameters M_0 and B_0 , the momentum and the buoyancy, respectively, added at the source ($z = 0$), described by the expressions

$$M_0 = 2\pi \int_0^{\frac{D_0}{2}} w^2 r dr \quad (7)$$

and

$$B_0 = 2\pi \frac{g}{\rho_\infty} \int_0^{\frac{D_0}{2}} w(\rho_\infty - \rho_0) r dr. \quad (8)$$

L_M characterises the vertical distance from the source where the momentum created by buoyancy forces surmounts the velocity momentum added at the source and the flow becomes buoyancy-dominated. In the considered plume experiment $B_0 = 0.01$ m⁴/s³ and $L_M = 0.0837$ m. Velocity and temperature profiles of self-preserving plumes are commonly described by Gaussian functions, where the pre-exponential factor and the exponent are determined by curve-fitting the experimental values. For the underlying experiments, this was done for vertical velocity and temperature profiles in the region of $6.5 < z/L_M < 16$, giving the following dimensionless correlations:

$$wB_0^{-\frac{1}{3}}z^{\frac{1}{3}} = 3.4e^{-58\eta^2} \quad (9)$$

and

$$g\beta\Delta TB_0^{-\frac{2}{3}}z^{\frac{5}{3}} = 9.4e^{-68\eta^2}. \quad (10)$$

In Equations (9) and (10), $\eta = r/z$ represents the self-similarity variable and ΔT denotes the excess temperature $T - T_\infty$. Within the analyses, the profiles given by Equations (9) and (10) deduced from experiments are compared with respective numerical results.

2.2.2 Numerical setup

The described experiments are analysed with OpenFOAM's (Version 1.6) *chtMultiRegionFoam* solver (without conjugated heat transfer), applying both the standard and the buoyancy-augmented k - ε model. An axis-symmetric set up with a domain size of 3 m in axial and 1 m in radial direction is employed (see Figure 2). Results are shown for the grid consisting of 10 uniform cells at the source and 70 cells with an expansion ratio of 6 for the remaining cells in radial direction. In the axial direction, 200 cells are equally distributed. In order to ensure grid-independent results, a coarse and a fine grid are considered in addition, with 40 x 100 and 160 x 400 cells, respectively. An adjustable time step is used to keep the Courant number close to 0.3. For the boundary conditions at the open boundaries of the domain, *zeroGradient* for velocity and *buoyantPressure* for pressure are prescribed at the side and *inletOutlet* with zero as inlet value for velocity and the *fixedValue* of 101325 Pa for pressure are considered at the top (see [8] for details on employed BCs). Values for k and ε are set to $1.7 \cdot 10^{-5} \text{ m}^2/\text{s}^2$ and $2.7 \cdot 10^{-6} \text{ m}^2/\text{s}^3$, respectively, at the source, assuming a turbulent intensity of $Tu_0 = 0.5 \%$ [10] and a turbulent mixing length $l_m = D_0/15 = 0.0042 \text{ m}$ [5]; $k = 10^{-6} \text{ m}^2/\text{s}^2$ and $\varepsilon = 10^{-9} \text{ m}^2/\text{s}^3$ are used for the ambient. Default settings for the discretisation schemes, i.e, upwind for convection and central-differencing for diffusion terms, as well as the default options for the solver are considered. To obtain a steady-state solution, a transient calculation is conducted with a total simulation time of 1200 s. The simulations using the buoyancy-augmented turbulence model are initialised with the converged solution of the standard k - ε model.

2.2.3 Results and discussion

Figures 3 and 4 show the obtained numerical results for vertical velocity and buoyancy in non-dimensional form at an axial position of $z = 1.4 \text{ m}$. It is worth to mention that in the area of self-preserving conditions profiles of different axial positions coincide. This behavior is also reproduced by the simulation.

As expected, the results obtained with the standard k - ε model significantly over-predict peak values and underestimate plume widths, for both velocity and buoyancy. On the

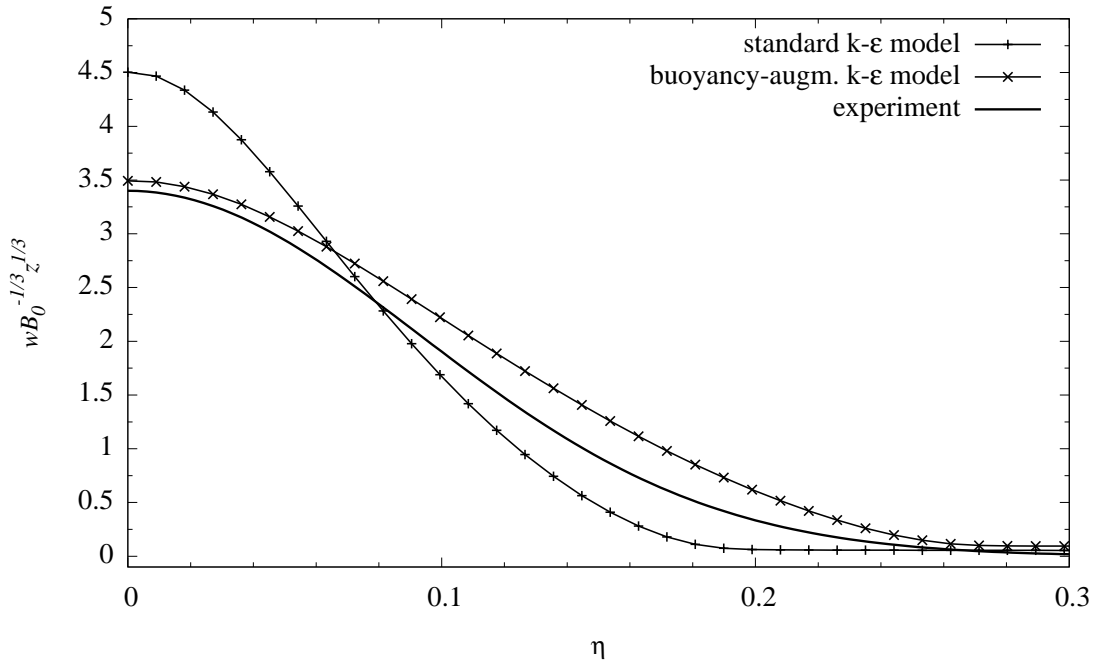


Figure 3: Non-dimensional vertical velocity profile

other hand, the predictions with the buoyancy-augmented turbulence model show excellent agreement with the plume correlations. Hence, the modified turbulence model can be used in the current implementation.

3 THE RADIATION MODEL

The two radiation models implemented in OpenFOAM (P1 and fvDOM) are investigated by simulating two benchmark problems: (i) two parallel, infinitely long black and diffuse walls with an emitting and absorbing gray medium in-between and (ii) an emitting and absorbing gray medium in a 2D rectangular enclosure. Numerical results are compared with analytical solutions available in [11] and [1], respectively.

3.1 Governing equations of the P1 and fvDOM model

The equations of the two models are given for gray, non-scattering gases and diffuse and gray surfaces. In case of the P1-model, a partial differential equation (PDE) of the form

$$\nabla \left(\frac{1}{a} \nabla G \right) = a(G - 4\sigma_{SB}T^4) \quad (11)$$

is solved for the incident radiation $G(\mathbf{x})$. Within the fvDOM-model, the solid angle is divided into discrete directions \mathbf{s} and for each of these directions the PDE of the radiative transfer equation (RTE), reading

$$\nabla(\mathbf{s}I) = a(I_b - I), \quad (12)$$

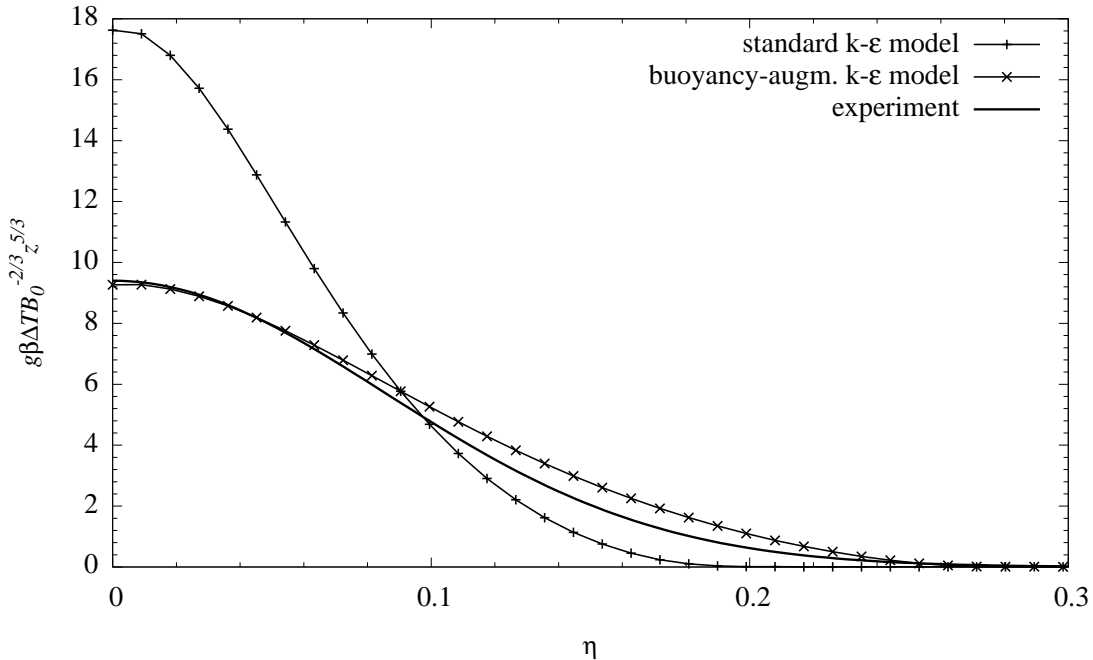


Figure 4: Non-dimensional mean buoyancy profile

is solved with respect to the radiative intensity $I(\mathbf{x}, \Omega)$, applying the approach of finite volume discretisation. The incident radiative energy is then calculated as

$$G(\mathbf{x}) = \int_{4\pi} I(\mathbf{x}, \Omega) d\Omega. \quad (13)$$

In both models, G is used to compute the divergence of the radiative heat flux vector \mathbf{q}_R which represents the radiative contribution to the energy equation, reading

$$-\nabla \cdot \mathbf{q}_R(\mathbf{x}) = a(G - 4\sigma_{SB}T^4). \quad (14)$$

3.2 Application – benchmark tests

3.2.1 Benchmark test 1: gray medium between two parallel (infinitely long) walls

The setup used for this simple test case is depicted in Figure 5, showing two black diffuse walls of T_1 and T_2 (with $T_1 < T_2$) at a distance D . The participating gray medium contributes only by absorption and emission with constant and homogeneous absorption/emission coefficient. The analytical solution for this problem is taken from [11]. The numerical simulations are performed in 2D with OpenFOAM’s *buoyantSimpleRadiationFoam*. A grid-sensitivity analysis suggested a spatial discretisation of 40 x 40 cells for both radiation models. The sensitivity analysis with respect to the solid-angle discretisation for the fvDOM-model shows satisfactory results with 24 discrete rays. In the analysis, top and bottom boundaries are defined as symmetry planes. For the two

walls, a *fixedValue* temperature BC with T_1 and T_2 , as well as *MarshakRadiationFixedT* and *greyDiffusiveRadiation* for G (P1-model) and I (fvDOM-model), respectively, are prescribed together with unit emissivity (see [8] for details on applied BCs). Convection is eliminated by setting the gravitational acceleration to $\mathbf{g} = (0 \ 0 \ 0)$ and by switching off the turbulence model. Conduction is deactivated by setting the Prandtl number to infinity, finally yielding a zero enthalpy diffusivity.

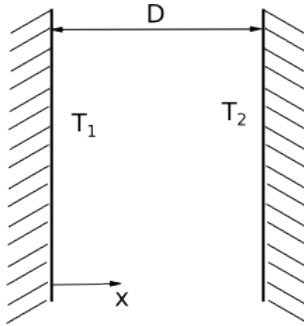


Figure 5: Configuration for benchmark test of a gray medium between two parallel, infinitely long walls

Temperature distributions are depicted in Figure 6 in dimensionless form, using

$$\Phi_b = \frac{T(x)^4 - T_2^4}{T_1^4 - T_2^4}, \quad (15)$$

for various values of optical thickness $\kappa_D = aD$. The solid lines correspond to the simulation whereas the symbols refer to the analytical solution. Both models show good agreement with the analytical results. Slight deviations from the analytical solution can be observed for optically thin media using the P1-model. This is well known for cases where collimated irradiation is present (see, e.g., [6]). The fvDOM-model predicts the temperature profiles more accurately. However, for the highest optical thickness $\kappa_D = 10$, it was necessary to solve the RTE after each flow iteration instead of after each tenth in order to obtain accurate results.

The wall-heat flux represents an important quantity when it comes to predicting the heat transfer from the fluid to the solid wall realistically. This quantity is shown in Figure 7 in dimensionless form, using

$$\Psi_b = \frac{q_R}{\sigma_{SB}(T_1^4 - T_2^4)}, \quad (16)$$

for different values of optical thickness κ_D . In case of the P1-model, the wall-heat flux is determined as

$$q_R = \frac{\varepsilon}{2(2 - \varepsilon)}(4\sigma_{SB}T_w^4 - G). \quad (17)$$

It is obvious that the heat flux of the two side walls has to be equal at the state of radiative equilibrium. However, the P1-model predicts different heat fluxes for the two

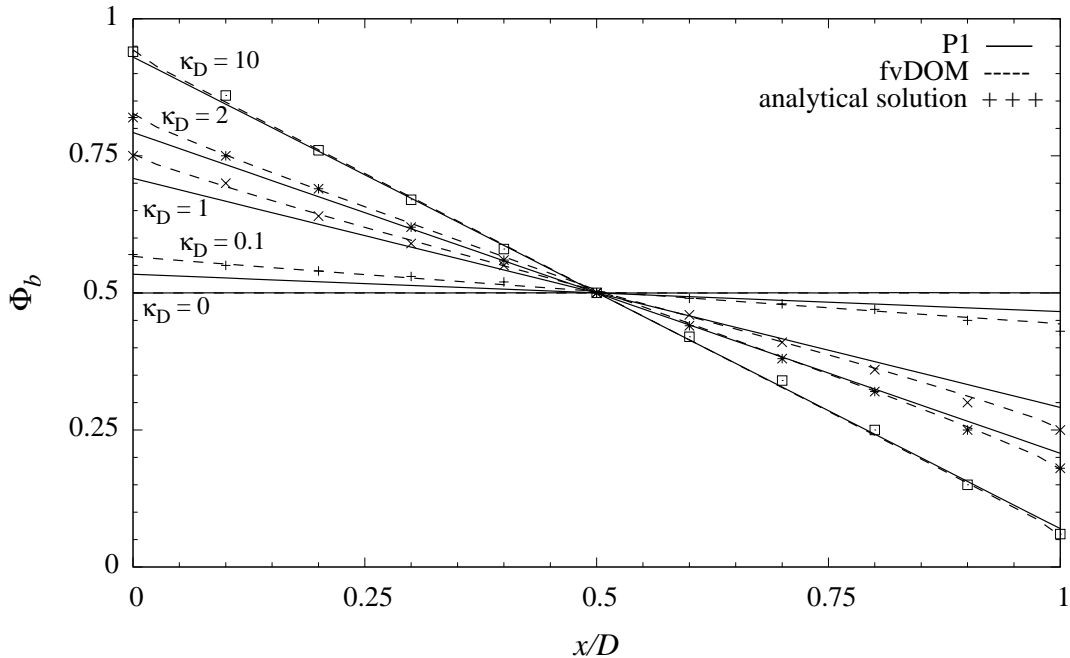


Figure 6: Temperature distributions using the P1- and fvDOM-model for different values of κ_D

walls as shown in Figure 7. The difference increases slightly with optical thickness. On the other hand, the fvDOM-model produces a heat flux of negligible differences between the two walls. Although small discrepancies between numerical and analytical results can be observed for increasing optical thickness, the results are much more accurate than those obtained with the P1-model, showing very good agreement with the analytical solution.

3.2.2 Benchmark test 2: gray gas in 2D rectangular enclosure

In the following, the test case of a rectangular medium exposed to diffuse radiation $I_D = 1 \text{ W/m}^2$ at the top of the domain is studied (see Figure 8). The absorbing and emitting medium is characterised by a constant and homogeneous absorption/emission coefficient. The 2D simulation is conducted with OpenFOAM's *buoyantSimpleRadiationFoam*. A sensitivity analysis with respect to grid size and solid angle discretisation suggested a constant grid size in all coordinate directions of 0.0125 m for both radiation models and 24 discrete rays for the fvDOM-model. All surfaces are assumed black and isothermal with $T_w = 1 \text{ K}$, except for the top-wall where the temperature is set to $T_w = (\pi I_D / \sigma_{SB})^{\frac{1}{4}} = (\pi \cdot 1 / 5.67 \cdot 10^{-8})^{\frac{1}{4}} = 86.28 \text{ K}$. BCs for G are *MarshakRadiation* and for I *greyDiffusiveRadiation*. The numeric results are obtained with constant optical thickness in vertical direction $\kappa_{z_0} = az_0 = 1$ and different aspect ratios $r = 2y_0/z_0$ in order to investigate the influence of changing geometries. The vertical temperature distribution in non-dimensional form in the center of the enclosure at $y = 0$ (Figure 9), using

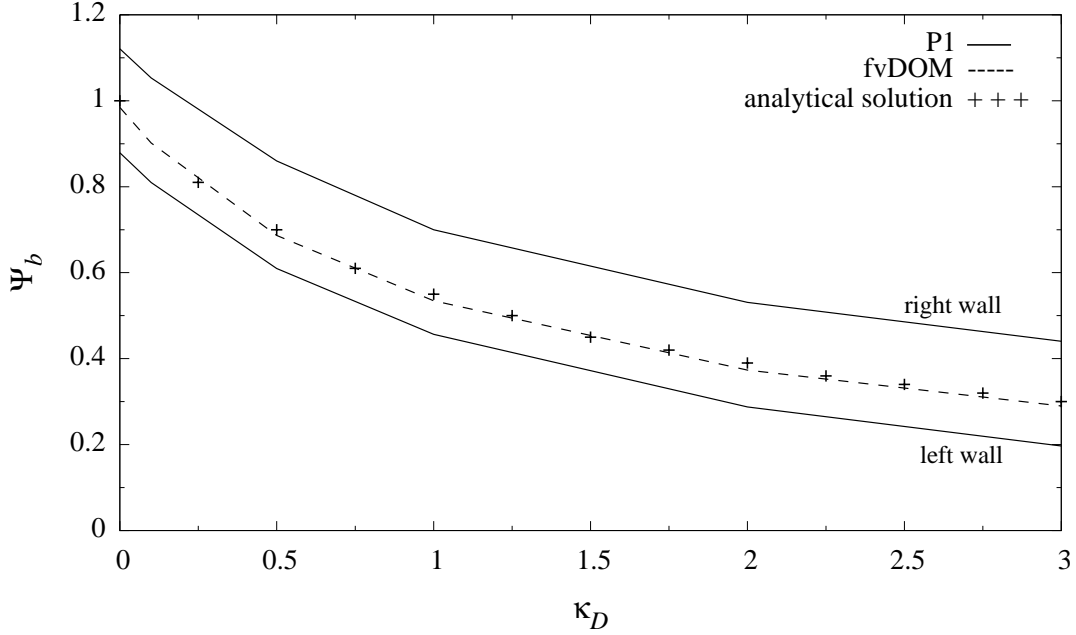


Figure 7: Radiative wall-heat flux as a function of κ_D using the P1- and fvDOM-model

$$\Phi_b = \frac{\sigma_{SB}T(z)^4}{\pi I_D}, \quad (18)$$

and the non-dimensional heat flux along the side and bottom wall (Figure 10 and 11), using

$$\Psi_b = \frac{q_R}{\pi I_D}, \quad (19)$$

are plotted and compared with data presented in [1], where the integral equation for radiative transfer in the 2D configuration is solved numerically by removing the singularity, yielding accurate results. As already observed in the previous example, results produced with the fvDOM-model are more accurate than the results obtained with the P1-model. It is worth mentioning that the numerical results mainly deviate from the results given in [1] in the region close to the prescribed radiation. These differences are greater with decreasing aspect ratio.

Figures 10 and 11 present heat fluxes at the side and bottom wall, respectively. The distributions obtained with the fvDOM-model correspond very well with those given in [1]. The profile along the bottom wall shows small oscillations for $r = 0.1, 0.5,$ and 1 which can be attributed to the so-called *ray effect*, a well-known deficiency of the fvDOM-model (see, e.g., [9]). As seen in the previous test case, the P1-model has problems in predicting wall-heat fluxes. The heat flux along the side wall is strongly over-estimated, especially for aspect ratios greater than 0.1, whereas results for the bottom-flux agree well with the results given in [1].

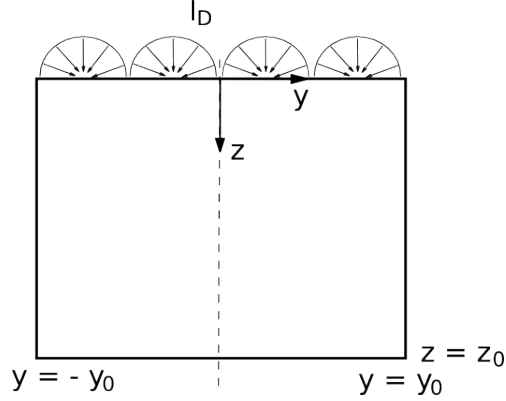


Figure 8: Geometry and coordinate system of rectangular medium exposed to diffuse radiation [1]

4 THE COMBUSTION MODEL

For the considered application, a simple combustion model to describe non-premixed combustion is needed. The model should be able to reproduce the heat release of the fire and its form (to conclude on a radiating surface of the flame) with reasonable accuracy. No resolution of detailed chemical processes is necessary. In the following, the combustion model used by OpenFOAMS's *fireFoam* solver is studied by simulating experiments on buoyant diffusion flames presented in [4]. Numerical results are also compared with correlations presented in [3].

4.1 Governing equations

The combustion model implemented in OpenFOAMS's *fireFoam* applies the mixture-fraction approach using infinitely fast chemistry, i.e., chemical reactions are faster than the time scales for diffusion and flow. Thus, combustion takes place as soon as fuel and oxidizer meet. The mixture fraction Z is a passive scalar defining the local fuel/oxidizer ratio as

$$Z = \frac{sY_f - Y_o + 1}{1 + s}, \quad (20)$$

where Y_f and Y_o are the mass fractions of fuel and oxidizer, respectively, and s is the stoichiometric air-fuel mass ratio. Z satisfies the respective transport equation, reading

$$\frac{\partial}{\partial t} (\rho Z) + \frac{\partial}{\partial x_j} (\rho u_j Z) = \frac{\partial}{\partial x_j} \left(\rho \mathcal{D} \frac{\partial Z}{\partial x_j} \right). \quad (21)$$

The boundary conditions for Z are unity in the fuel stream and zero in the oxidizer stream. Additionally, a similar transport equation for Y_f is solved, reading

$$\frac{\partial}{\partial t} (\rho Y_f) + \frac{\partial}{\partial x_j} (\rho u_j Y_f) = \frac{\partial}{\partial x_j} \left(\rho \mathcal{D} \frac{\partial Y_f}{\partial x_j} \right) + R, \quad (22)$$

with the fuel-consumption rate R as source term, which is modelled as

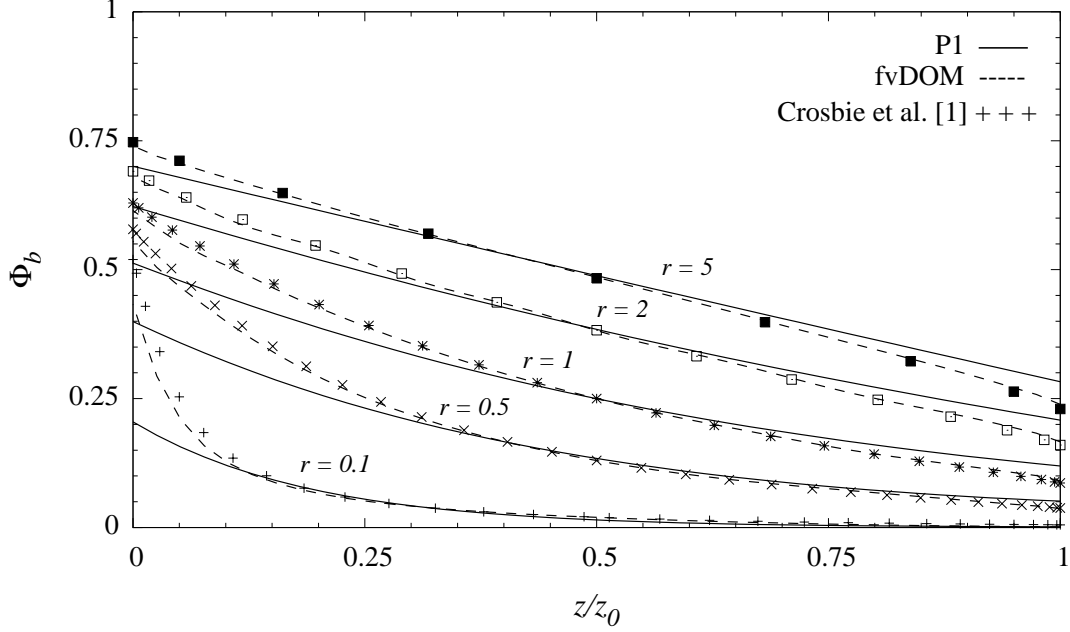


Figure 9: Temperature distributions in the center of the domain using the P1- and fvDOM-model for different values of r

$$R = \frac{\rho}{\Delta t C_C} \min(Y_f, \frac{Y_o}{s}). \quad (23)$$

In Equation (23), Δt denotes the time step and C_C is a model constant. Diffusion coefficients \mathcal{D} are equal for all species and set to the effective thermal diffusivity assuming a unit Lewis number. Z and Y_f allow then to determine Y_o (Equation (20)) and therefore the mass fraction of combustion products ($= 1 - Y_f - Y_o$). The contribution of the combustion process to the energy equation is given by the combustion source term, reading

$$q_C = -R\Delta h_C, \quad (24)$$

where Δh_C is the heat of combustion of the fuel.

4.2 Numerical simulation

In the considered experiments [4], velocity and temperature were measured in the flame of a natural gas (mainly methane) burner with a square section of 0.3 m x 0.3 m. The amount of escaping gas was varied to simulate five different burning rates. Velocity and temperature profiles at the center-line of the domain in the flame, intermittent and plume region, are given by [4]

$$\frac{w}{Q^{1/5}} = k \left(\frac{z}{Q^{2/5}} \right)^n \quad (25)$$

and

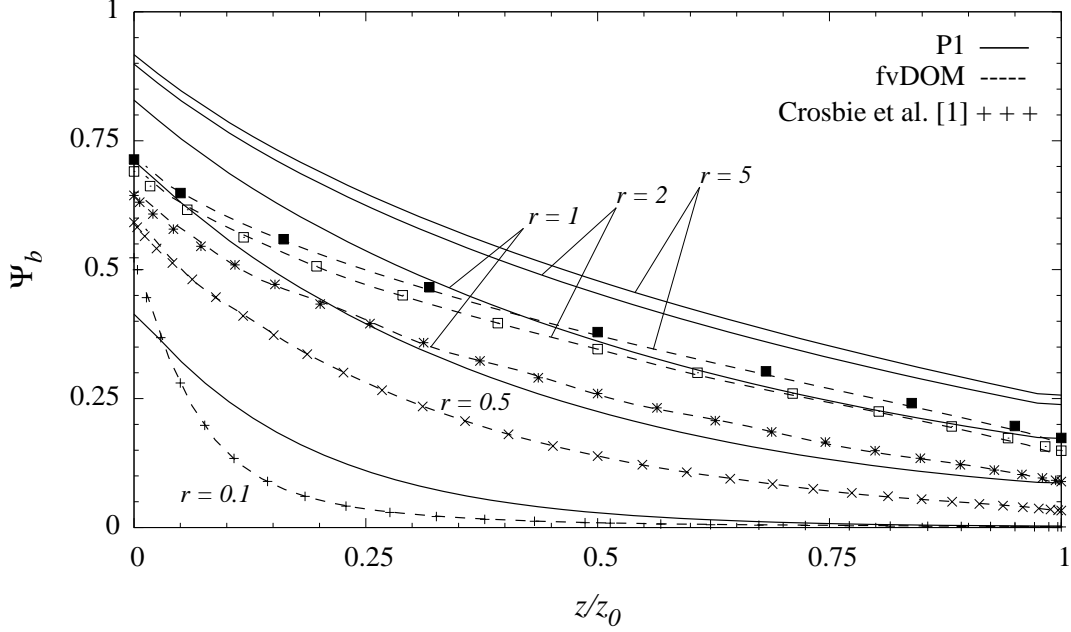


Figure 10: Heat flux at side wall using the P1- and fvDOM-model for different values of r

$$\frac{2g\Delta T}{T_\infty} = \left(\frac{k}{C}\right)^2 \left(\frac{z}{Q^{2/5}}\right)^{2n-1}. \quad (26)$$

In Equations (25) and (26), $C = 0.9$ whereas the parameters k and n vary depending on the region. Numerical data for center-line temperatures are also compared with the relationship presented in [3] for the intermittent and plume region, reading

$$\frac{\Delta T}{T_\infty} = C_T(1 - X_r)^{\frac{2}{3}} \left(\frac{z - z_0}{D^*}\right)^{-\frac{5}{3}}, \quad (27)$$

with $C_T = 9.1$ and $X_r = 0.2$ [4], where the latter describes the radiative fraction of the fire's heat release. z_0 is the location of the virtual origin of the fire plume, calculated as

$$\frac{z_0}{D^*} = 1.37 - 1.02 \frac{D_0}{D^*}, \quad (28)$$

where D^* is the characteristic plume diameter, given by

$$D^* = \left(\frac{Q}{\rho_\infty c_p T_\infty \sqrt{g}}\right)^{\frac{2}{5}}. \quad (29)$$

For the 3D simulation with *fireFoam*, methane is used as fuel. One quarter of the experimental set-up is considered and the symmetry planes are realised by respective cyclic boundary conditions (see Figure 12). Furthermore, a circular inlet is used since the shape of the burner has little effect on flame properties in case of the same cross-sectional area as

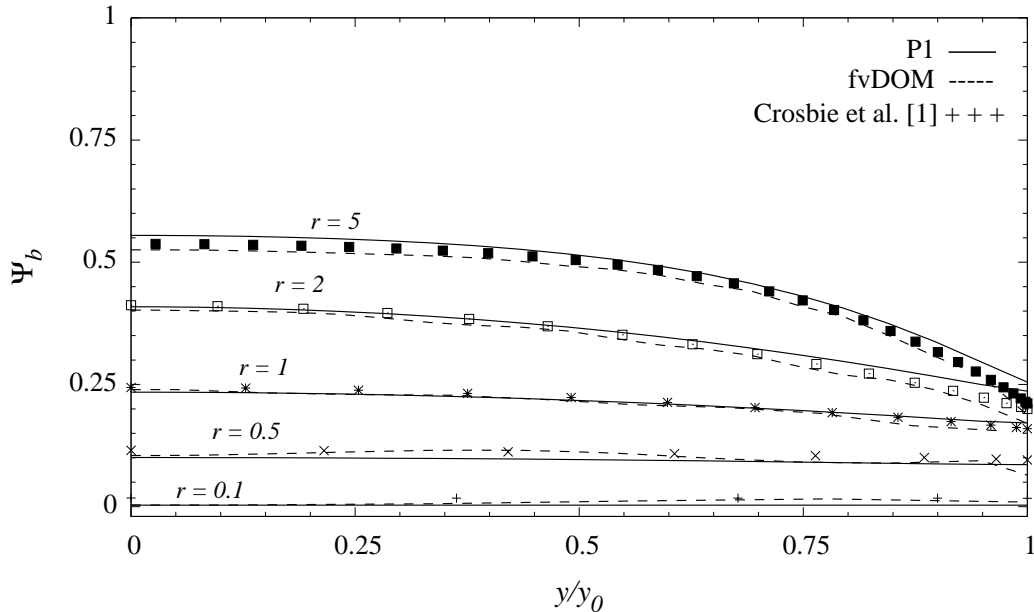


Figure 11: Predicted heat flux at bottom wall using the P1- and fvDOM-model for different values of r

the square opening [2]. The computational domain measures 3 m in axial and 1 m in radial direction with an inlet diameter D_0 of 0.34 m. Results are shown for a grid consisting of 48 cells at the burner inlet and 336 cells for the remaining horizontal area. 150 cells are equally distributed in axial direction. In order to guarantee grid-site-independent results, two additional grids of size 108 x 75 cells and 1536 x 300 cells are studied. To model the different burning rates of 15, 25, 35, 45 and 55 kW, the mass-flux (applied via the BC-type *flowRateInletVelocity*) is varied at the inlet assuming a heat of combustion of $\Delta h_C = 5 \cdot 10^7$ J/kg. The BCs for Z and Y_f are set to unity at the fuel inlet, *zeroGradient* at the floor and zero for the remaining boundaries. The fuel enters at ambient temperature of $T_\infty = 293$ K. Default settings for the discretisation schemes and default options for the solver are considered. Radiation is not enabled and the standard k - ε model is used to account for turbulence.

4.3 Results and discussion

Figures 13 and 14 show comparisons of center-line temperature and vertical velocity with the respective distributions presented in [4]. Hereby, an over-estimation of the peak values is observed, which can be attributed to the insufficient description of buoyancy effects by the standard k - ε model. Additionally, no radiative heat transfer is considered in the simulation leading to higher flame temperatures and velocities due to missing radiative heat loss. Furthermore, no radiation correction for the thermocouple data was used in [4]. Therefore, the experimental results underestimate the actual gas temperature.

The combustion model is not able to predict a constant temperature distribution in the

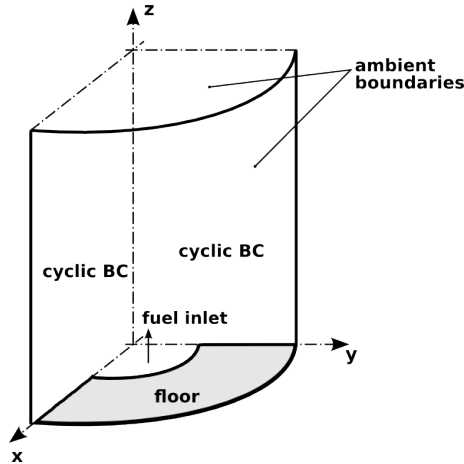


Figure 12: Computational domain for the simulation of the gas-burner experiment

flame region (up to $z/Q^{2/5} < 0.08 \text{ m/kW}^{2/5}$). A direct transition from the flame to the plume region ($z/Q^{2/5} > 0.2 \text{ m/kW}^{2/5}$) is observed for the temperature without indication for an intermittent region, whereas this can be seen for the vertical velocity but at different points. In the flame and plume region, the respective slopes for the velocity distribution correspond well with the experimental correlations. For the temperature, this is mainly true in the plume region.

Figure 15 shows the distribution of the center-line temperature for a burning rate of $Q = 15 \text{ kW}$ compared with the relationship presented in Equation (27) [3]. Similar conclusions as above can be drawn. Hence, deeper investigation of combustion parameters (e.g. C_C) as well as the influence of radiation and buoyancy effects is necessary.

5 Conclusions and outlook

A CFD-tool for the simulation of fire events in enclosures was developed in OpenFOAM. A buoyancy-augmented $k-\varepsilon$ model based on the *General Gradient Diffusion Hypothesis* was implemented in OpenFOAM's *chtMultiRegionFoam* solver, showing good agreement with experimental data. In order to study the applicability of the two radiation models P1 and fvDOM, two benchmark tests were performed exhibiting satisfactory agreement between numerical results and analytical solutions for the fvDOM-model. Finally, a combustion model applying the mixture-fraction approach was considered to simulate non-premixed combustion. Comparison of the numerical results with experimental data indicated the need for further investigation on the influence of model parameters, radiation and buoyancy effects.

Future work will include the incorporation of the modified $k-\varepsilon$ model, the fvDOM radiation model and the combustion model into one solver allowing to simulate real-scale fire tests. Furthermore, pyrolysis and soot modeling will be added to enlarge the applicability of the code, which will finally be able to realistically determine the surface temperatures of fire-loaded structures.

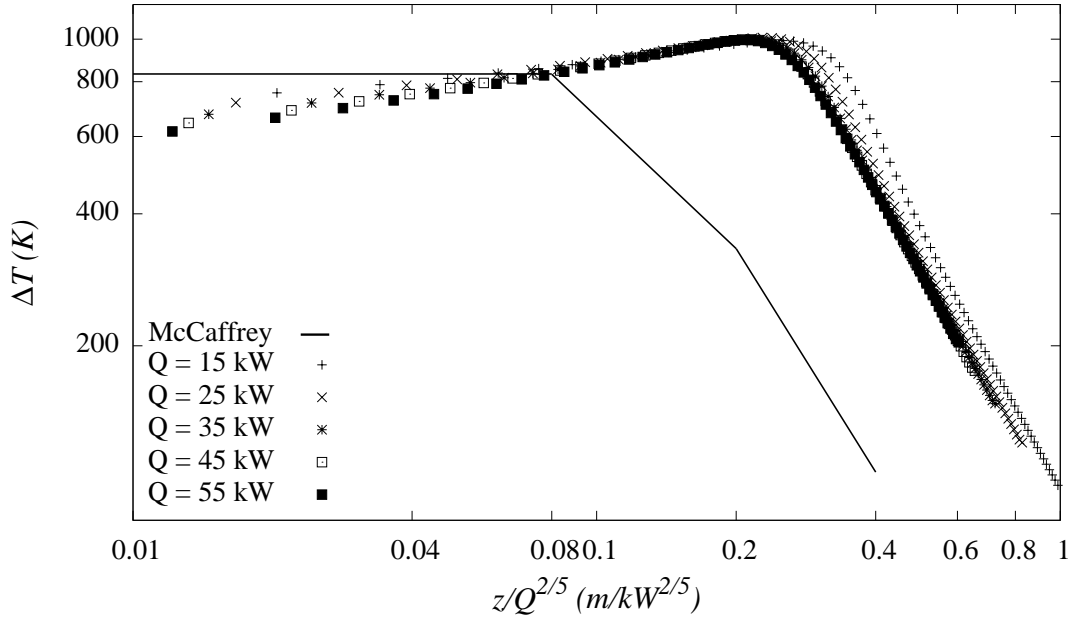


Figure 13: Center-line temperature for different burning rates Q

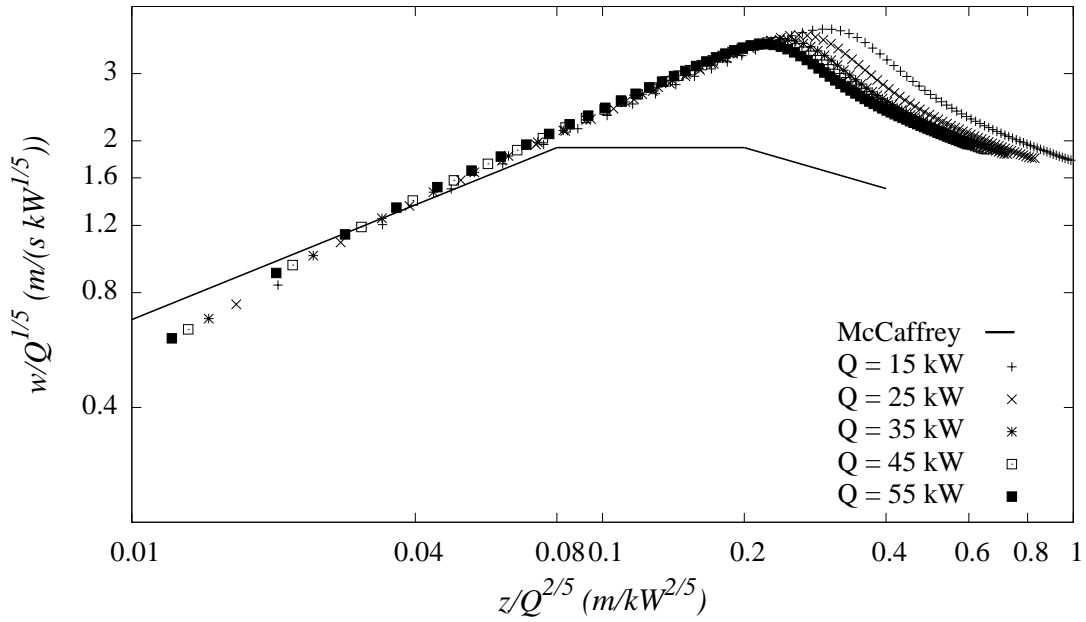


Figure 14: Distribution of scaled vertical velocity along the center-line for different burning rates Q

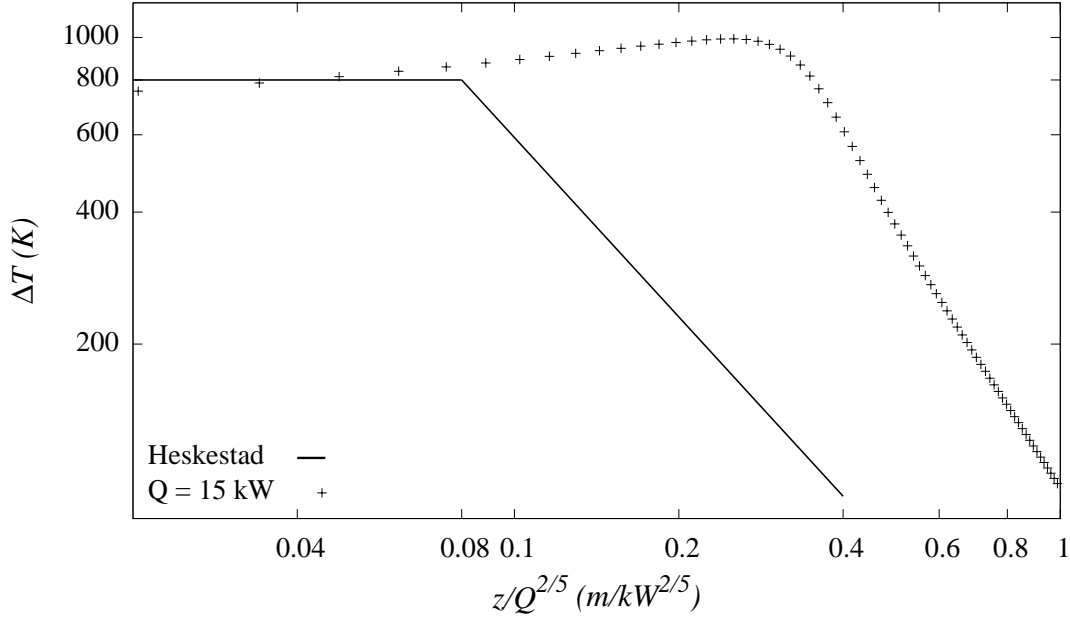


Figure 15: Center-line temperature for $Q = 15 \text{ kW}$ compared with Equation (27) [3]

References

- [1] A. L. Crosbie and R. G. Schrenker. Radiative transfer in a two-dimensional rectangular medium exposed to diffuse radiation. *Journal of Quantitative Spectroscopy & Radiative Transfer*, 31(4):339–372, 1984.
- [2] Y. Hasemi and T. Togunaga. Flame geometry effects on the buoyant plumes from turbulent diffusion flames. *Fire Science and Technology*, 4(1):15–26, 1984.
- [3] G. Heskestad. *Fire Plumes. SFPE Handbook*. National fire protection association, 2nd edition, 1995.
- [4] B.J. McCaffrey. Purely buoyant diffusion flames: some experimental results. Report NBSIR 79-1910, National Bureau of Standards, Washington D.C., 1976.
- [5] B. Merci, E. Dick, J. Vierendeels, and C. Langhe. Determination of ε at inlet boundaries. *Int Journal of Num Methods for Fluid & Heat Flow*, 12(1):65–80, 2002.
- [6] M. Modest. *Radiative Heat Transfer*. Academic Press, 2nd edition, 2003.
- [7] S.M. Olenick and D.J. Carpenter. An updated international survey of computer models for fire and smoke. *Journal of Fire Protection Engineering*, 13(2):87–110, 2003.

- [8] OpenCFD Limited. *OpenFOAM 1.6 - The Open Source CFD Toolbox - User Guide*, 2009.
- [9] M. A. Ramankutty and A. L. Crosbie. Modified discrete-ordinates solution of radiative transfer in three-dimensional rectangular enclosures. *Journal of Quantitative Spectroscopy & Radiative Transfer*, 60(1):103–134, 1998.
- [10] A. Shabbir and W.K. George. Experiments on a round turbulent buoyant plume. *Journal of Fluid Mechanics*, 275:1–32, 1994.
- [11] R. Siegel and J. Howell. *Thermal Radiation Heat Transfer*. Taylor & Francis, 4th edition, 2002.
- [12] K. van Maele and B. Merci. Application of two buoyancy-modified k- ϵ turbulence models to different types of buoyant plumes. *Fire Safety Journal*, 41:122–138, 2006.
- [13] K. William and Jr. George. Turbulence measurements in an axisymmetric buoyant plume. *International Journal of Heat and Mass Transfer*, 20:1145–1154, 1977.